Matrix Isolation Fourier Transform Infrared and Ab Initio Studies of the 193-nm-Induced Photodecomposition of Formamide

J. Lundell,*,† M. Krajewska,†,‡ and M. Räsänen†

Laboratory of Physical Chemistry, University of Helsinki, P.O. Box 55 (A.I.Virtasen aukio 1), FIN-00014 University of Helsinki, Finland

Received: February 11, 1998; In Final Form: May 19, 1998

Ultraviolet irradiation of formamide in solid argon forms hydrogen-bonded, carbon- and oxygen-attached complexes NH_3−CO and NH_3−OC. Computationally, the carbon-attached complex is 1.2 kJ mol^{-1} more stable than the oxygen-attached complex. However, a thermal equilibrium of the two structures is found experimentally in the matrices. Moreover, the oxygen-attached complex dominates in the 193-nm-induced photolytic complex formation from formamide. In xenon matrices, the photochemistry of formamide increasingly yield the HNCO+H_2 binary system. The change in photochemistry of formamide between the argon and xenon enviroments can be attributed to an external heavy-atom effect, where xenon enhances the rate of intersystem crossing from a singlet to a triplet surface.

Introduction

The amide group has long been of practical importance and of fundamental interest because it is the repeat unit in both biologically important macromolecules and industrially important polymeric materials. The smallest model molecule of the peptide prototype NH−C═O linkage is formamide. To understand the properties of the two important functional groups C═O and NH_2 in peptides, knowledge of the molecular properties of formamide is crucial in structure−activity relationships in organic and physical chemistry.

Experimentally, the structure of formamide has been studied by microwave spectroscopy,[1−4] electron diffraction,[5] and by analysis of vibrational−rotational spectral data.[6] The vibrational properties of formamide have been studied by IR and Raman spectroscopy in the gas phase[7−9] and in low-temperature rare gas, nitrogen, and CO matrices.[10,11] Along with the rapid development of computer hardware, several theoretical studies of the ground-state properties of formamide have been published,[12−24] predicting structural and vibrational properties.

In general, the structure of formamide has been well characterized but the planarity of the molecule has been under strong debate. The microwave data were initially interpreted to indicate either a planar or a nonplanar structure for formamide until Hirota and co-workers showed that the molecule is planar.[4] Later, analysis of the vibrational−rotational spectrum indicated the same conclusion.[6] Computationally, the shallow NH_2 torsional potential has been even more of a problem. Recently, the planarity of formamide was shown by high-level CCSD-(T)/pVTZ calculations by Fogarasi and Szalay.[24] They found that when correlation calculations are coupled with the use of correspondingly large basis sets, in which the higher angular momentum functions are crucial, the final result is an exactly planar formamide molecule. For more complete discussion of computational approaches on the formamide planarity, the reader is directed to ref 24.

From the photochemical point of view, knowledge of excited electronic states is essential. Five bands have been identified in the electronic absorption spectrum of formamide.[25−27] A weak n → π^* transition, labeled as the W band, at 219 nm (5.8 eV) that merges to an intense $\pi \rightarrow \pi^*$ absorption (V_1) below 169 nm. The recent vacuum ultraviolet (VUV)-electron-energy-loss spectroscopy experiments by Gingell et al.[27] places this latter absorption at ≈7.36 eV. Additionally, two Rydberg states have been identified at 185 nm (R_1) and at 159 nm (R_2), and the next singlet excited state, the Q band, at 135 nm. The lowest triplet states have been observed at 5.2, ∼ 6.0, and 6.4 eV.[27]

Several computational studies of the UV absorption spectrum of formamide have become available.[12,28−33] Generally, the variety of MRCI calculations place the first and the second excited singlet states in their correct energetic places compared with the experimental results. Also, four intervening Rydberg states have been found by computation between the first and second excited states. The properties of formamide in the two lowest lying excited states and the first excited triplet state have been mapped by Li and co-workers, using CIS-level of theory,[34] who found that all three of these excited states (S_1, S_2, and T_1) have a nonplanar equilibrium structure. In all these states, the primary excitation occurs from the formamide ground state within the carbonyl moiety, resulting in a buildup of electron density on the carbon atom. This buildup can be observed as the pyramidal carbonyl group typical for n → π^* excited carbonyl compounds.[35]

In this paper, we will review the formamide structure computationally using the 6-311++G(2d,2p) basis set with MP2 electron correlation, as well as the density functional theory enabling the Becke3-LYP hybrid functional. These levels of calculations will be useful when we reassess part of the observed vibrational spectrum of formamide in rare gas matrices. The single-electron excitation (CIS-MP2) calculations are used to trace the excited states of formamide to aid the interpretation of experimental photochemical observations. The main focus will be the photochemistry of formamide under 193 nm laser irradiation in low-temperature matrices.

* Corresponding author. E-mail: lundell@csc.fi.
† Laboratory of Physical Chemistry.
‡ Permanent address: Institute of Chemistry, University of Wroclaw, F. Joliot-Curie 14, 50−383 Wroclaw, Poland.

S1089-5639(98)01072-X CCC: $15.00
Published on Web 07/29/1998

Experimental Details

The vapor pressure of formamide is too low to allow the compound to be handled by usual vacuum line methods. The matrix was prepared by flushing a small amount of molecular sieves that were wetted with formamide with the matrix gas under reduced pressure. The gas mixture thus formed was sprayed onto the cold CsI window kept at 18 K in a Displex DE−202E closed-cycle cryostat. Accurate matrix ratios could not be obtained, but we estimate the ratios to be between 500 and 1000. The deposition conditions (speed of deposition, temperature of formamide during flushing, temperature of the cold window) were optimized to achieve minimal amount of associates in the matrix.

The spectra were recorded on a Nicolet 60 SX FTIR (Fourier transform infrared) spectrometer, which typically coadded 200 interferograms. The spectrometer was usually run at 0.25 cm^{-1} resolution in the spectral region 400−4000 cm^{-1}.

The photolysis source for the experiments was an excimer laser (Estonian Academy of Sciences, ELI-76) operating at 193 nm (ArF). Typically, the pulse energies were between 15 and 25 mJ, and the irradiation area on the cold window was ≈3 cm^2.

Computational Details

All calculations were performed within the framework of the GAUSSIAN 94[36] package of computer codes using the second-order perturbation theory (MP2).[37,38] The DFT exchange functional used to study the formamide molecular properties was the Becke hybrid method[39,40] based on the standard Becke 1988 exchange functional.[41] This functional includes the Slater exchange along with corrections involving the gradient of the electron density (nonlocal exchange). The hybrid functional includes contributions also from the Hartree−Fock exchange and DFT exchange-correlation, and have been determined as three parameter functionals fitted to various atomic properties. The correlation functional was the gradient-corrected functional by Lee, Yang, and Parr (LYP).[42] The notation proposed by Pople and co-workers,[43] where X−C represents the exchange and correlational functionals, respectively, can be used to write the whole DFT functional as Becke3-LYP. The harmonic wavenumbers were calculated analytically both at the MP2 and Becke3-LYP levels.

The electronically excited states of formamide were studied with the configuration interaction with all single excitations included, and with a correction for the electron correlation to the CIS energies (CIS-MP2).[44] All excited singlet and triplet surfaces shown are calculated using a frozen ground-state structure of formamide, and the C−N bond distance was scanned following vertical single electron excitation.

The applied basis sets were the standard split-valence, 6−311-type Gaussian basis functions[45,46] added with diffuse[47] and polarization[48] functions on all atoms to give the 6-311++G-(2d,2p) basis set.

All calculations were carried out on CRAY C94 and SGI PowerChallenge supercomputers at the CSC-Center for Scientific Computing Ltd. (Espoo, Finland).

Results and Discussion

Formamide Precursor. The equilibrium geometries of formamide calculated at the MP2 and Becke3-LYP levels are shown in Table 1. For the MP2 level, the planar and nonplanar symmetry results are included. The nonplanarity of formamide has been discussed in detail previously,[14,18−20,23,24] and we will address it here only briefly. Generally, the planar structure is obtained at HF-level using large Gaussian basis sets. The inclusion of electron correlation for the Gaussian-type orbitals results in a nonplanar structure with a slightly pyramidal amino group. Florian and Johnson[23] noted also that the B-LYP level follows the structure and energetics at the MP2 level using equivalent basis sets. Nevertheless, at all correlated levels, the energy difference between the planar and the nonplanar structure is much less than the zero-point energy of the out-of-plane wagging vibration of the NH_2 group. At the MP2/6-311++G-(2d,2p) level of theory, the energy difference between the planar and nonplanar structure is 0.24 J mol^{-1}. Qualitatively, the molecule can be considered a planar system with a shallow single-minimum potential. This result is also derived from microwave measurements,[4] vibration−rotation spectra,[6] and high-level ab initio calculations.[24]

TABLE 1: Equilibrium Structures[a] of Formamide at the MP2 and Becke3-LYP Levels of Theory Employing the 6-311++G(2d,2p) Basis Set

bond	microwave[b]	MP2 planar	MP2 nonplanar	Becke3-LYP
C−O	1.219	1.2168	1.2167	1.2113
N−C	1.352	1.3587	1.3593	1.3578
H_1−N	1.002	1.0026	1.0028	1.0064
H_2−C	1.098	1.0974	1.0974	1.1032
H_3−N	1.002	1.0000	1.0002	1.0037
O−C−N	124.7	124.76	124.75	124.79
H_1−N−C	118.5	119.24	119.05	119.37
H_2−C−N	112.7	112.58	112.59	112.59
H_3−N−C	120.0	121.04	120.82	121.29
O−C−N−H_1	0.0	0.0	−4.25	−0.069
H_2−C−N−H_1	0.0	0.0	3.54	0.0

[a] The bond distances are given in Ångströms and the angles are given in degrees. The hydrogens in formamide are numbered as follows: H_1 is the hydrogen in cis position from the C═O bond, H_2 is the hydrogen in the formyl group, and H_3 is the hydrogen in the trans position from the C═O bond. [b] The microwave data are from ref 4.

The MP2- and Becke3-LYP-calculated bond distances and bond angles of formamide agree well with the experimental results. Comparing DFT and MP2 results it can be noted that bond distances for both hydrogens are slightly longer at the DFT level. Simultaneously, the C═O and C−N bonds are shorter at the Becke3-LYP level than at the MP2 level. The bond angles are predicted to be almost equal for MP2 and Becke3-LYP compared with the experimental average structure.[4]

The vibrational properties of formamide at the MP2 and the Becke3-LYP levels of theory and in low-temperature matrices are presented in Table 2. Comparing the vibrational frequencies between the nonplanar and planar structures at the MP2 level, only insignificant differences are found except in the NH_2 wagging mode. As a transition state on a shallow potential energy surface, one eigenvalue of the planar structure is negative. The Becke3-LYP calculated spectrum is qualitatively similar to the MP2 results. Both MP2 and Becke3-LYP predict the C═O and C−N stretchings and the NH_2 wagging mode to be the most intense absorptions in the formamide spectrum. This prediction is also in accordance with experimental results both in the gas phase and in low-temperature matrices.[7−11] The interpretation of the vibrational spectrum in the 300−700 cm^{-1} region has been discussed extensively in the literature. Originally the 303 cm^{-1} absorption in solid argon[11] was assigned as the NH_2 torsion according to HF/4-31G calculations. Nevertheless, calculations at the MP2 level using larger basis sets[20,22] have shown that the 682 cm^{-1} absorption is due to the torsional mode, and the original assignment had inverted assignments because of the low-level calculations used. The

TABLE 2: Calculated and Observed Vibrational Spectra (in cm^{-1}) of Formamide[a]

assignment[b]	MP2 planar	MP2 nonplanar	Becke3-LYP	argon[c]	krypton[c]	xenon[c]
ν_{as} NH_2	3790.4 (63)	3787.8 (62)	3724.4 (45)	3548	3549	3535
ν_s NH_2	3640.8 (54)	3639.2 (53)	3586.5 (35)	3427	3426	3411
ν CH	3029.6 (82)	3029.8 (82)	2950.0 (93)	2884	2864	2851
ν C═O	1777.9 (418)	1778.0 (414)	1782.1 (441)	1740	1739	1731
δ NH_2	1630.7 (48)	1631.0 (47)	1623.4 (58)	1579	1576	1574
δ CH	1440.1 (7)	1440.0 (7)	1419.2 (7)	1400	1395	1389
ν CN	1278.9 (118)	1278.8 (118)	1266.4 (115)	1261	1270	1248
(r) NH_2 rock	1056.6 (8)	1060.4 (7)	1055.5 (6)	1047	1052	1052
(γ) CH oop def.	1053.1 (5)	1050.4 (5)	1038.2 (3)	1035	1027	1025
τ NH_2	636.5 (12)	635.0 (13)	636.9 (13)	682	698	705
δ OCN	570.0 (10)	569.8 (9)	569.8 (11)	564	571	567
NH_2 wag	−72.3 (220)	124.3 (224)	169.6 (209)	303	313	316

[a] In all calculations, the 6-311++G(2d,2p) basis set was used; the numbers in parentheses are the relative intensities expressed in km mol^{-1}. [b] Following the assignments in ref 22. [c] From ref 11, except the NH_2 rocking and CH out-of-plane deformation modes (see text for details).

TABLE 3: Observed Absorptions after 193-nm-Induced Photodecomposition of Formamide in Argon and Xenon Matrices[a]

argon	xenon	assignment	argon	xenon	assignment
3607.9	3607.8			1661.8	
3594.3 −				1618.9	
				1615.7 +	NH_3 (+CO)
3561.0	3518.3			1589.1	
	3479.9	HNCO (+H_2)			
	3464.6			1162.0	HXeH
3417	3412.1	NH_3 (+CO)		1058.3	*
	3374.5			1044.7	*
	3354.2			1040.5	*
3325.2			1031.0		
3296.8 −	3284.7	NH_3 (+CO)	974.3	1015.2 +	NH_3 (+CO)
3284.0				1011.4 +	
	3194.4			995.0	
	3165.1			954.2	$(XeHXe)^+$
3181.4	3133.1	NH_3 (+CO)		843.0	$(XeHXe)^+$
	3127.2			815.8	*
	3079.0			764.4	HNCO (+H_2)
2265.7	2267.3	HNCO (+H_2)		731.2	$(XeHXe)^+$
2263.9	2260.1			573.7	HNCO (+H_2)
2259.2	2254.4				
	2195.0				
2145.9	2154.8 +				
2143.9	2148.3 +				
	2138.6	CO (+NH_3)			
	2133.3	CO mon.			
	2129.4				
2136.6	2124.2	CO (+NH_3)			
	2121.3				
2090.0	2087.4				
2048.5					

[a] Key: (−, +) decrease or increase, respectively, of the peak intensity upon annealing; (*) very weak absorptions that could be due to HOCN from the photoinduced isomerization of HNCO.

high-level ab initio calculations also point out one additional discrepancy between the calculated and observed vibrational spectrum of formamide.

In low-temperature matrices, a weak NH_2 rocking mode is assigned at 1185 cm^{-1} in argon, at 1195 cm^{-1} in krypton, and at 1196 cm^{-1} in xenon. In nitrogen and carbon monoxide matrices, this absorption has been assigned at 830 and 909 cm^{-1}, respectively. This kind of matrix shift seems very large and, in fact, according to the high-level calculations in the literature[22,23] and the calculations presented in this paper, this absorption should have much lower frequency than that reported from the rare gas matrix data. The spectral region between 1000 and 1300 cm^{-1} in different rare gas matrices is shown in Figure 1. In all matrices, a doublet at ≈1180 cm^{-1} exists. Now the intensities of these two bands, compared with the strong C−N stretching absorption, are much weaker than in the literature

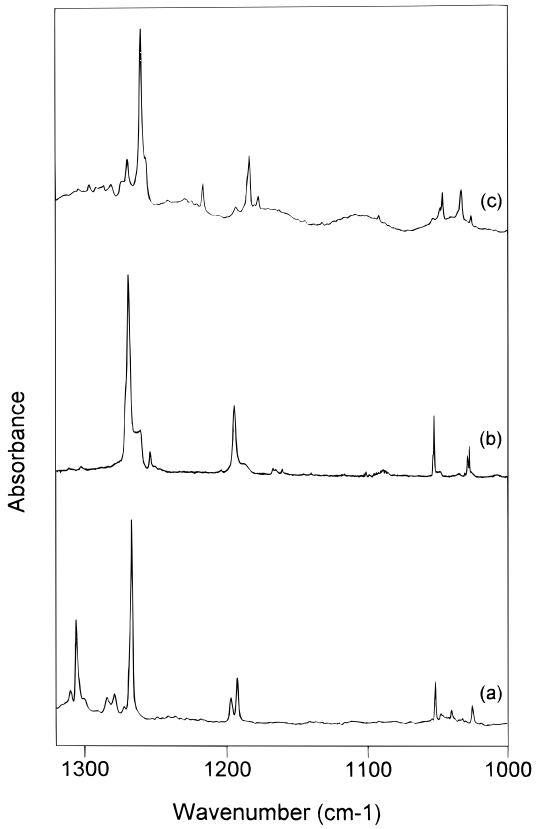

Figure 1. The infrared spectra of formamide in the 1000−1320 cm^{-1} spectral region: (a) in xenon, after deposition at 20 K; (b) in krypton, after deposition at 15 K; (c) in argon, after deposition at 18 K.

spectra.[11] Therefore, the C−N stretching absorption at ≈1260 cm^{-1} and the doublet cannot be from the same molecule because the experimental conditions were practically identical in these experiments as in the previous experiments. We believe that the doublet at ≈1180 cm^{-1} is due to the C−N stretching of formamide dimer present in the matrix. This assignment would also agree with the IR frequencies given by Itoh and Shimanouchi[9] for the formamide crystal showing two bands at 1133 and 1140 cm^{-1}. The bands due to the NH_2 rock can be found in Figure 1 as well. In all rare gas matrices, a pair of absorptions at ≈1050 cm^{-1} is observed. Aided by the MP2/6-311++G(2d,2p) calculated vibrational spectrum, we assign the higher wavenumber component as the NH_2 rocking mode, and the lower wavenumber absorption as the CH out-of-plane deformation. The additional weak absorptions in this region are due to different sites of formamide monomer and associated species.

Photochemistry of Formamide in Argon. The 193-nm-

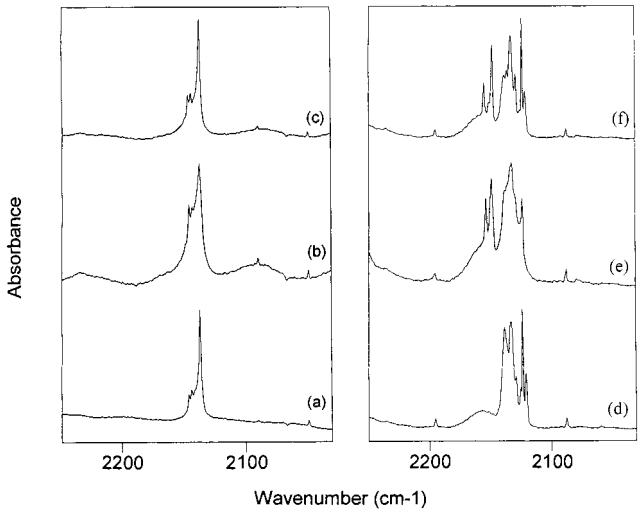

Figure 2. The CO stretching region in argon (left) and xenon (right) matrices: (bottom) after 193 nm irradiation of the formamide precursor; (middle) the spectra measured during annealing cycles at 30 and 50 K in argon and xenon, respectively; (top) spectra measured after annealing cycles at ≈20 K.

irradiated formamide produces in Ar vibrational bands that are typical for ammonia and carbon monoxide. In the CO stretching region a strong band at 2136.6 cm^{-1} is observed with two smaller sidebands at 2143.9 and 2145.9 cm^{-1}. All of these bands are shifted from the CO monomer absorption in Ar at 2138.6 cm^{-1}.[49] The reversible temperature dependence of these absorptions can be seen in Figure 2 a−c.

Ammonia has been studied in CO matrix by Hagen and Tielens,[50] and the vibrational bands of NH_3 were found to be strongly shifted from their positions in rare gas matrices. The complex between NH_3 and CO has never been specifically studied by infrared (IR) spectroscopy, but the structure of the complex has been determined by microwave spectroscopy in molecular jets.[51] From the rotational spectra of NH_3−CO and its different deuterated congeners, it was concluded that the CO monomer is attached from the carbon end to the nitrogen atom of ammonia. Also, it was suggested that the complex does not involve hydrogen bonding.[51] However, ab initio calculations on the NH_3−CO complex show that two different hydrogen-bonded structures, NH_3−CO and NH_3−OC, are found on the complex potential energy surface.[52] The calculated, BSSE-corrected interaction energies of the carbon-attached NH_3−CO and oxygen-attached NH_3−OC complexes are −3.26 and −2.03 kJ mol^{-1}, respectively, calculated at the CCSD(T)/6-311++G-(3df,3pd)//MP2/6-311++G(3df,3pd) level of theory.[52] The interactions between NH_3 and CO are very weak, and of similar magnitude as typical van der Waals interaction energies of rare gas atoms. Therefore, the interactions with the matrix environment are crucial for the stabilization of the weak complex in the matrix, and they strongly influence the prevalence of different complex structures within the matrix cage.[52] The assignment of both NH_3−CO and NH_3−OC complexes existing in the matrix will be emphasized and discussed in detail in the context of experiments in Xe matrices later.

In the ammonia vibrational spectrum, the ν_2 mode is the strongest. After UV irradiation of the precursor, only one strong absorption at 974.3 cm^{-1} is seen. In the work of Süzer and Andrews,[53] the ν_2 absorption of monomeric NH_3 was reported to be at exactly same wavenumber as that observed here. Abouaf-Marguin and co-workers[54] in their extensive work on NH_3 in rare gas matrices found two bands near this position: The $R(0_0^-)$ band at 971 cm^{-1} and the $Q(1_1^-)$ band at 974.5 cm^{-1}. In CO matrix, the ν_2 mode of ammonia was identified at 981.0 cm^{-1}.[50]

In the ν_4 region of NH_3 (at ≈1630 cm^{-1}) only very weak absorptions are found after UV photolysis, and nothing conclusive can be said about the observed absorptions can be. However, it must be noted that these bands are between the values reported for monomeric NH_3 in solid Ar (1638.9 cm^{-1})[54] or CO matrix (1625.3 cm^{-1}).[50]

In the NH-stretching region, new weak absorptions after UV photolysis were observed at 3181.4, 3284.0, 3296.8, 3325.2, 3417.0, 3561.0, 3594.3, and 3607.9 cm^{-1}. The 3181.4 and 3561.0 cm^{-1} absorptions are quite sharp, whereas the others are much broader. The NH_3 absorptions in solid CO are broad in the temperature range 10−20 K.[50] Also, the broadness in the ammonia bands is most likely due to the NH_3 rotation in the matrix cage at the temperatures used in the experiments. In solid CO, the ν_1 absorption of ammonia was assigned at 3320.3 cm^{-1}, and the ν_3 absorption at 3427.8 cm^{-1}.[50] In Ar, these absorptions are shifted to higher wavenumbers than the values in CO matrix; that is, 3345.5 and 3447.3 cm^{-1}, respectively.[53,54]

Complex formation in the cage is mainly evidenced by the perturbed CO-stretching absorption. The NH_3 absorptions are very little shifted from their positions in unperturbed matrices. The method of preparation of the 1:1 complex is very straightforward and it relies on at least partial cage effect preventing hot fragments from escaping. It gives well-defined species because the photoproducts are trapped in the original precursor site in the matrix. Secondary photoproducts are possible because NH_3 has the $\tilde{A} \leftarrow X$ absorption in the 170−220-nm region.[55] This excitation should lead to NH_2 (X^2B_1) and hydrogen atoms. However, no NH_2 radicals could be observed. The observed photodecomposition of formamide in solid Ar resembles the 193-nm photochemical pathways of formic acid in Ar, where the $S_1 \leftarrow S_0$ excitation produces mainly ground-state H_2O+CO 1:1 complexes.[56,57]

Photochemistry of Formamide in Xenon. The photodecomposition of formamide in Xe seems to be much more complicated than in solid Ar (or solid krypton, which resembles Ar). The photoinduced decomposition of formamide versus the appearance of the photoproducts is shown in Figures 3 and 4. In Xe, the major dissociation channel of $HCONH_2$ leads preferentially to HNCO+H_2 instead of NH_3+CO. However, traces of the NH_3+CO complexes can be found as already noted. The CO and NH_3 absorptions show more components in Xe than in Ar. This result can be seen in Figure 2, where the CO fundamental band after photodecomposition of formamide is compared in Ar (Figure 2 a−c) and Xe (Figure 2 d−f) matrices. In Xe, two multiplets with a broad absorption due to NH−CO are observed after 193-nm laser irradiation. The lower frequency sharp doublet is assigned according to the data in Ar matrices to the oxygen-attached, hydrogen bonded NH_3−OC complex. The broader multiplet is very close to the monomeric CO absorption in solid Xe (2133.2 cm^{-1} [49]), and we believe that during photodissociation, a small amount of free CO is formed in Xe. Upon annealing to 55 K, the NH_3−OC band decreases, the monomer band becomes broader, and new bands appear at higher wavenumbers from the monomer value. Based on the vibrational shifts, these bands are assigned as the carbon-attached, hydrogen-bonded complex NH_3−CO. The process of forming the carbon-attached complex upon annealing is similar to that observed for the H_2O−CO complexes. In solid Xe, after photodecomposition of formic acid,[56] the oxygen-attached H_2O−OC complex was the prevalent species compared with monomeric CO and the carbon-attached H_2O−CO complex. Upon

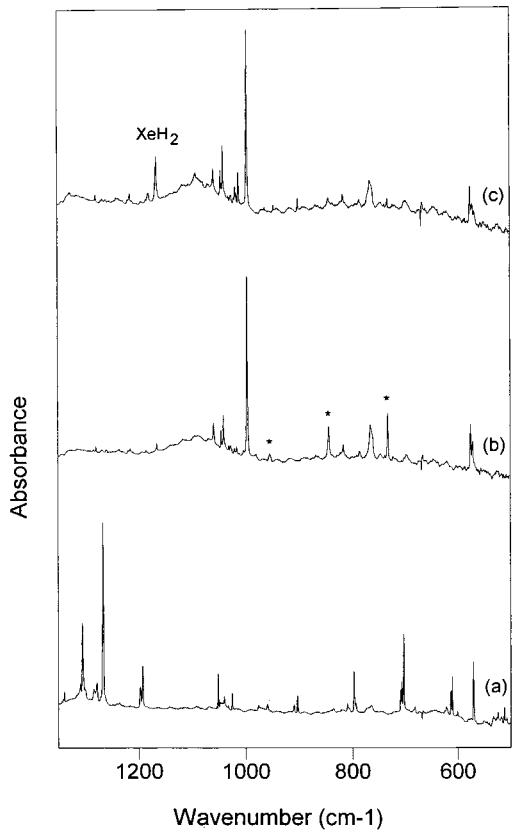

Figure 3. The disappearance of formamide versus the appearance of the photoproducts in the 500−1300 cm^{-1} region upon laser irradiation in solid xenon: (a) after deposition of formamide at 20 K; (b) after 2000 pulses of 193 nm laser irradiation; (c) after annealing cycles 25−55−25 K. The asterisks indicate the progression due to $(XeHXe)^+$.

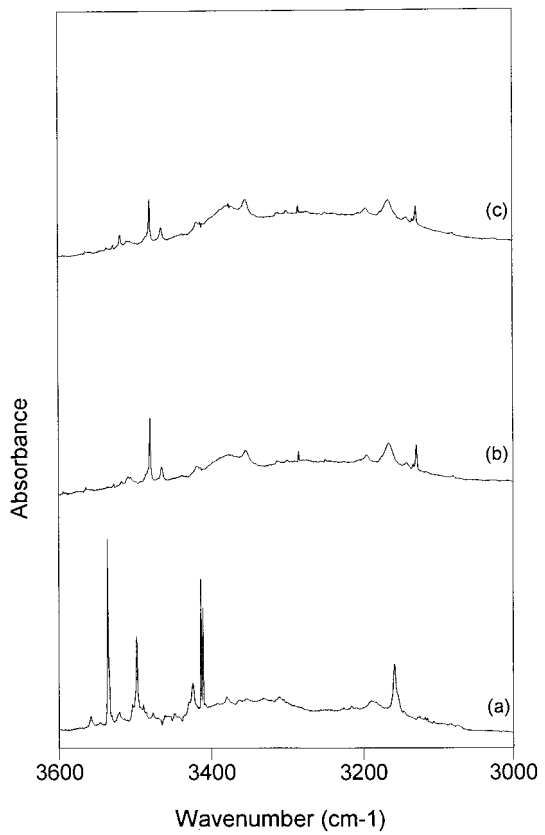

Figure 4. The disappearance of formamide versus the appearance of the photoproducts in the 3000−3600 cm^{-1} region upon laser irradiation in solid xenon. (a) after deposition of formamide at 20 K. (b) After 2000 pulses of 193 nm laser irradiation; (c) after annealing cycles 25−55−25 K.

annealing, the higher-energy H_2O-OC complex relaxed into the lowest-energy H_2O-CO complex. Similarly, here the main product after UV-induced decomposition of formamide is the oxygen-attached NH_3-OC complex. Upon annealing, the NH_3-OC complex can be partially transformed to NH_3-CO. However, cooling the matrix to 18 K after annealing cycles regenerates the original intensities of the complex species observed after the photodecomposition of the precursor. There clearly exists a thermal equilibrium between the two complex species. Moreover, the experimental evidence suggest that the oxygen-attached NH_3-OC complex is stabilized more than the NH_3-CO complex in the matrices, therefore also being the lowest-energy species. Also, in the double-doping experiments of NH_3 and CO in solid Ar, Dubost[49] found a band shifted +4.9 cm^{-1} from the monomer absorption. This absorption correlates with the NH_3-CO complex now identified both in Ar and Xe matrices in this study, and indicates that the calculated vibrational shifts used to identify the complexes can be trusted on a qualitative level. However, the temperatures used in this study (>18 K) enable rotation of ammonia in the matrix, which broadens the vibrational bands and thus lower temperature studies are planned.

Formation of Isocyanic Acid (HNCO). After 193 nm irradiation of the formamide/Xe sample, several bands belonging to HNCO could be detected. The NCO bending (ν_5) is observed at 573.7 cm^{-1}. No previous data on HNCO in Xe matrices is available, but several studies have reported vibrational frequencies for HNCO in Ar and neon matrices.[58−60] According to these studies, the NCO bending is found in Ar also at 573.7 cm^{-1}, showing no medium effects. The δ HNC mode (ν_4) was assigned in Ar at 769.8 cm^{-1}, and in Xe this band is a broad absorption at 764.4 cm^{-1}. Both ν_4 and ν_5 modes of HNCO involve a large contribution from the hydrogen motion,[60] and in the Xe cage these vibrational modes can sample a large variety of sligthly different structures giving rise to the broad absorptions observed.

The NCO asymmetric stretching mode (ν_2) is the strongest absorption in HNCO and is assigned at 2254.4 cm^{-1} in Xe, showing two weaker shoulders at 2260.1 and 2267.3 cm^{-1}. This intense absorption is even observable in our Ar experiments at 2259.2 cm^{-1}, even though only a very small amount of HNCO is present in the matrix after formamide photodecomposition. Previously this ν_2 mode of HNCO has been assigned at 2259.0 cm^{-1} in solid Ar.[60]

In the NH-stretching (ν_1) region, two absorptions are observed at 3464.6 and 3479.9 cm^{-1}. Winnewisser et al.[60] also reported a doublet for this mode in solid Ar at 3516.8 and 3505.7 cm^{-1} with equal intensities. In our Xe experiments, we find the higher wavenumber component to be much stronger than the lower wavenumber component. In Ar, the difference between the two absorptions is 11.1 cm^{-1}, whereas in Xe the difference is 15.3 cm^{-1}. Moreover, it must be noted that this mode is highly affected by the matrix environment, and the shifts from Ar to Xe are at ≈41 and ≈37 cm^{-1} for the higher and lower wavenumber components, respectively. The origin of the doublet structure of the N−H stretching band is well discussed by Winnewisser and co-workers,[60] and can briefly be noted to result from both almost free rotational motion of HNCO, which is coupled with the surrounding rare gas lattice, and Fermi resonance between the ν_1 band and the $\nu_2+\nu_4+\nu_5$ combination.

$HNCO+H_2$. In this context it must be emphasized that we believe that the two hydrogen atoms left over from the

photoinduced decomposition of formamide form a H_2 molecule also trapped in the same Xe cage with the HNCO molecule. This approximation would be consistent with the photodecomposition of formic acid producing $CO_2 + H_2$ in the Xe matrix,[56,57] where CO_2 bandshifts due to H_2 could be found. In the present study it is impossible to evaluate the influence of H_2 on the spectrum of HNCO because of the lack of unperturbed wavenumbers. Nevertheless, the cage effect of trapping all photoproducts in the cage is not completely valid because, as can be seen in Figure 3, small traces of $XeHXe^+$ and HXeH can still be found after laser photolysis.

The formation of monomeric CO in Xe displays the cage-exit differences between Xe and Ar. Neutral hydrogen atoms are trapped in Xe in the form of HXeH, as evidenced by the 1162 cm^{-1} absorption[61] that is still present after photodissociation of formamide. Also, some amount of $(XeHXe)^+$ centers are formed,[62] as seen by the progression starting at 731 cm^{-1} and marked with asterisks in Figure 3. If the neutral H atoms diffuse and meet NH_2 radicals, NH_3 should be formed. However, if monomeric NH_3 is formed, it also absorbs the 193 nm irradiation by decomposing, finally producing a NH radical and ejecting two neutral hydrogen atoms.[55] Therefore, the existence of monomeric ammonia in these matrix experiments is highly improbable, explaining the formation of the ultimate hydrogen trap in Xe matrices; that is xenon dihydride (XeH_2).[61]

Photochemistry of NH_3 in solid Xe deserves a few additional comments. In the case of H_2O-CO, it was found that the water subunit does not decompose when complexed with CO in low-temperature matrices.[57] However, when water is isolated in the matrix, it can be decomposed by 193 nm laser light.[61,63] Similarly for the NH_3-CO complexes, the interaction with CO can enhance relaxation of the pumped energy, whereas the NH_3 monomer decomposes under similar conditions.

HNCO+H_2 versus NH_3+CO. The differences between formamide photolysis in Ar and Xe can be explained by the similarity with the photochemistry of formic acid.[56,57] In solid Ar, the $n \rightarrow \pi^*$ excitation leads to the first excited singlet state, where a radical pair HCO + NH_2 is formed. The hot HCO radical donates the hydrogen to the NH_2 radical forming NH_3, and finally yields hydrogen-bonded NH_3+CO complexes as described previously.[52] In Xe, the $n \rightarrow \pi^*$ excitation occurs at 193 nm photolysis as well. However, when the radical pair is formed in the excited state, a strong external heavy-atom effect due to Xe is present, which induces intersystem crossing to a triplet surface yielding HNCO+H_2. A schematic picture of these suggested processes is shown in Figure 5. The possible involvement of external heavy atom effect was suggested in photochemistry of vinyl formate in matrices.[64]

To test the validity of these mechanistic aspects we studied the excited states of formamide by CIS-MP2/6-311++G(2d,-2p) calculations. All other structural parameters were kept at their equilibrium values (MP2/6-311++G(2d,2p)), and only the C−N bond distance was scanned mimicking the bond breaking upon 193 nm photochemistry. The calculated singlet and triplet surfaces are plotted in Figure 6. It can be noted that only the first excited singlet state (S_1) and the two lowest triplet states are within the energy of the photons at 193 nm (6.42 eV). All these states seem to be bound, but upper states intervene with them producing avoided crossings in the 1.7−2.0 Å region upon stretching the C−N bond. According to these calculations, it seems highly possible to have a $T \leftarrow S_1$ intersystem crossing (ISC) activated in solid Xe. Further theoretical studies would be valuable to determine which of the two triplet states is responsible for the formation of the HNCO+H_2 binary system.

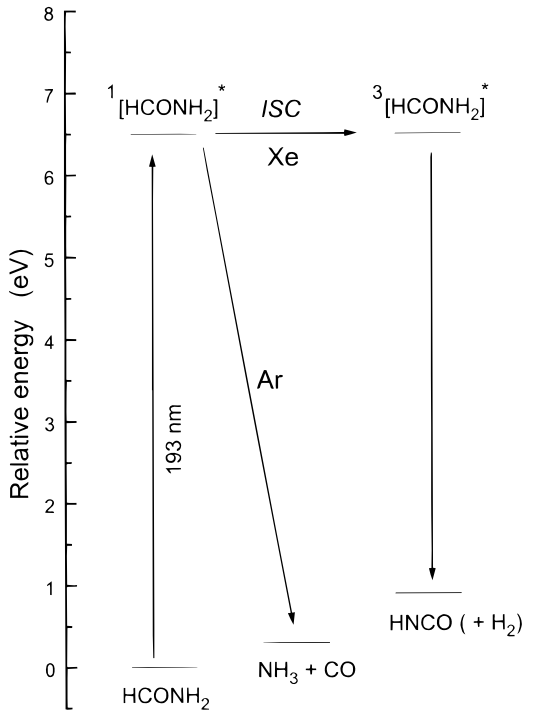

Figure 5. A schematic picture of the photochemistry of formamide following the 193 nm laser irradiation in low-temperature argon and xenon matrices.

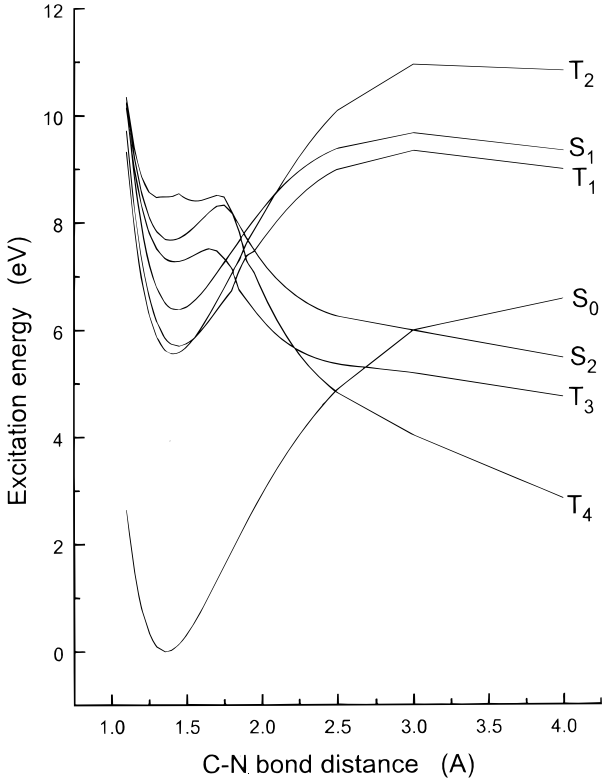

Figure 6. The CIS-MP2/6-311++G(2d,2p) calculated excited states of formamide along the C−N bond. All other structural parameters were kept constant at their equilibrium (MP2/6-311++G(2d,2p)) values. The energy of the 193-nm photon used in the experiments is 6.42 eV.

To probe the ISC in solid Xe, we performed experimental studies doping Ar matrices of formamide with Xe. The relative formation of different photoproducts can be seen in Figure 7. The lowest trace in Figure 7 shows the photoproducts after 193 nm photodecomposition of formamide in pure Ar matrix. Clearly the CO absorption is much more intense than the ν_2

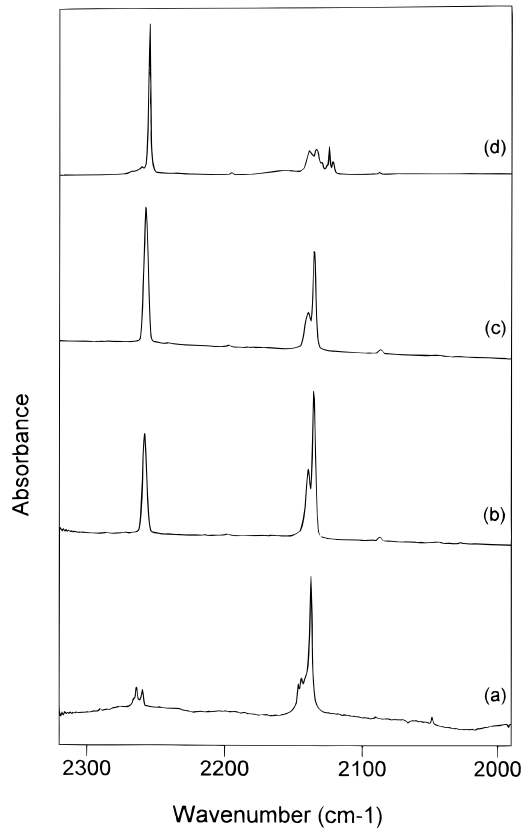

Figure 7. The photoproduct ratios after 193-nm-induced photodecomposition of formamide in (a) Ar, (b) 90% Ar + 10% Xe, and (c) 80% Ar + 20% Xe, and Xe matrices.

band of HNCO shown as a doublet at ≈2260 cm^{-1}. When 10% Xe is introduced into the matrix, the ν_2 band of HNCO becomes comparable to the CO absorption. With 20% Xe in the formamide/Ar matrix, the intensities of these two bands are already inverted, indicating a larger shift of the photochemistry from the S_1 surface to a triplet surface. In pure Xe matrices, the CO absorption appears much weaker than the NCO ν_2 band of HNCO. These double-doping experiments show that when the probability of finding a Xe atom in the matrix cage beside the formamide monomer increases, the probability of forming HNCO+H_2 binary system increases. In fact, Pimentel and coworkers[65] showed that only one Xe atom in the rare gas cage next to the (dimethylamino)benzonitrile precursor is sufficient to increase the ISC rate to a triplet surface.

Secondary Photochemical Reactions. HNCO has a broad absorption spectrum at 180−280 nm.[65] At 180 nm there is the S_1 ($^1A''$) ← S_0 ($^1A'$) transition to the lowest excited singlet state close to the thresholds of the spin-allowed dissociation channels: (1) H (^2S) + NCO (X $^2\Pi$) and (2) NH (a $^1\Delta$) + CO (X $^1\Sigma^+$). In the gas phase, these dissociation channels are used as a convenient photolytic source for NCO and NH radicals.[66] In Ar matrix, Milligan and Jacox[58] showed that the matrix-isolated HNCO, irradiated below 224 nm, led to photoequilibrium between HNCO and cyanic acid (HOCN). Also, photodecomposition of HNCO to NH+CO could be found in the matrix.[58] However, a small amount of HNCO undergoes photoinduced reactions to form secondary products. An absorption at 3518.3 cm^{-1} in Xe can be tentatively assigned to the HOCN isomer. The ν_1 absorption of HOCN has been identified in solid Ar[60] at 3569.6 cm^{-1}, suggesting a shift of 51 cm^{-1} going from Ar to Xe. The strongest band of HOCN is the CN stretching mode assigned in Ar at 2286.3 cm^{-1}.[60] In our experiments, bands of HOCN in this spectral region would be strongly overlapped by the HNCO absorption. Additionally, the weak absorption at ≈1040 cm^{-1} could be tentatively assigned for HOCN, corresponding to the 1081.3 cm^{-1} absorption observed in Ar matrix.[60] Luminescence spectra on the photolysis will be employed to detect short-lived species encountered in studies that are in progress in our laboratory.

The third product channel found in the 193-nm-induced photodecomposition of HNCO is the NH+CO binary system. In the Xe matrix no NH absorptions could be identified but in the CO stretching region, the broad structure at ≈2160 cm^{-1} could be due to the NH+CO complex. The complex is estimated to be weak, explaining the broad absorption structure. Moreover, due to the characteristic shift of the CO fundamental, the complex should be a carbon-attached complex. An oxygen-attached complex would show a red shift from the unperturbed monomer value in the Xe cage. Nevertheless, it must be emphasized that only a very small amount of the photochemically formed HNCO decomposes further to give NH+CO binary system. Our preliminary results of using 248 nm laser irradiation to decompose formamide indicate a larger extent of photodecomposition of HNCO to give NH+CO as well HOCN due to photoisomerization process.[67]

Conclusions

The 193-nm-induced photodecomposition of formamide in low-temperature matrices leads to NH_3+CO and HNCO+H_2 products. In Ar matrices, the NH_3−CO binary systems dominate. Broad bands for the complex were observed, indicating weak interactions on a shallow potential energy surface. Two possible complex structures were suggested to exist in the matrix. Computationally these structures can be attributed to hydrogen-bonded, carbon- and oxygen-attached complexes NH_3−CO and NH_3−OC, respectively. Contrary to the expectations from the calculations, the higher-energy species NH_3−OC was the primary photoproduct possibly stabilized by interactions with the cage atoms.

In Xe matrices, the photodecomposition of formamide is changed due to external heavy atom effecs of the matrix atoms with the radical pair formed initially. The external heavy-atom effect increases the rate of ISC from the excited singlet state to a triplet state, leading to the increase of HNCO+H_2 as primary photoproducts. A small amount of NH+CO and HOCN+H_2 can be detected due to photoinduced reactions of HNCO. In solid Xe, XeH_2 is also found, indicating cage exit and the existence of neutral hydrogen atoms in the matrix after laser irradiation. The formation of hydrogen atoms in the matrix is attributed to photoinduced decomposition of ammonia in the matrix.

References and Notes

(1) Kurland, R. J. *J. Chem. Phys.* **1955**, *23*, 2202L.
(2) Kurland, R. J.; Wilson, E. B. *J. Chem. Phys.* **1957**, *27*, 585.
(3) Costain, C. C.; Dowling, J. M. *J. Chem. Phys.* **1960**, *32*, 158.
(4) Hirota, E.; Sugisaki, R.; Nielsen, C. J.; Sørensen, O. *J. Mol. Spectrosc.* **1974**, *49*, 251.
(5) Kitano, M.; Kichutsu, K. *Bull. Chem. Soc. Jpn.* **1974**, *47*, 67.
(6) Brown, R. D.; Godfrey, P. D.; Kleibömer, B. *J. Mol. Spectrosc.* **1987**, *124*, 34.
(7) Evans, J. C. *J. Chem. Phys.* **1954**, *22*, 1228.
(8) King, S. T. *J. Phys. Chem.* **1971**, *75*, 405.
(9) Itoh, K.; Shimanouchi, T. *J. Mol. Spectrosc.* **1972**, *42*, 86.
(10) Räsänen, M. Doctoral Thesis, University of Helsinki, 1983.
(11) Räsänen, M. *J. Mol. Struct.* **1983**, *101*, 275.
(12) Stenkamp, L. Z.; Davidson, E. R. *Theor. Chim. Acta (Ber.)* **1977**, *44*, 405.
(13) Bock, C. W.; Trachtman, M.; George, P. *J. Mol. Spectrosc.* **1981**, *89*, 76.

(14) Fogarasi, G.; Balazs, A. *J. Mol. Struct.* (THEOCHEM) **1985**, *133*, 105.
(15) Boggs, J. E.; Niu, Z. *J. Comput. Chem.* **1985**, *6*, 46.
(16) Jasien, P. G.; Stevens, W. J.; Krauss, M. *J. Mol. Struct. (THEOCHEM)* **1986**, *139*, 197.
(17) Wright, G. M.; Simmonds, R. J.; Parry, D. E. *J. Comput. Chem.* **1988**, *9*, 600.
(18) Østergård, N.; Christiansen, P. L.; Nielsen, O. F. *J. Mol. Struct. (THEOCHEM)* **1991**, *235*, 423.
(19) Østergård, N. Doctoral Thesis, The Technical University of Denmark, Lyngby, 1991; The Danish Center for Applied Mathematics and Mechanics, Report no. S57, 1991.
(20) Kwiatkowski, J. S.; Leszczynski, J. *J. Mol. Struct.* **1992**, *270*, 67.
(21) Wong, M. W.; Wiberg, K. B.; Frisch, M. J. *J. Am. Chem. Soc.* **1992**, *114*, 1645.
(22) Kwiatkowski, J. S.; Leszczynski, J. *J. Mol. Struct.* **1993**, *297*, 277.
(23) Florian, J.; Johnson, B. G. *J. Phys. Chem.* **1994**, *98*, 3681.
(24) Fogarasi, G.; Szalay, P. G. *J. Phys. Chem. A* **1997**, *101*, 1400.
(25) Basch, H.; Robin, M. B.; Kuebler, N. A. *J. Chem. Phys.* **1968**, *49*, 5007.
(26) Ballard, R. E.; Jones, J.; Read, D.; Inchley, A.; Cranmer, M. *Chem. Phys*. **1988**, *147*, 629.
(27) Gingell, J. M.; Mason, N. J.; Zhao, H.; Walker, I. C.; Siggel, M. R. F. *Chem. Phys.* **1997**, *220*, 191.
(28) Basch, H.; Robin, M. B.; Kuebler, N. A. *J. Chem. Phys.* **1967**, *47*, 1201.
(29) Harding, L. B.; Goddard, W. A. *J. Am. Chem. Soc.* **1975**, *97*, 6300.
(30) Nitzsche, L. E.; Davidson, E. R. *J. Chem. Phys.* **1978**, *68*, 3103.
(31) Oliveros, E.; Riviere, M.; Teichteil, C.; Malrieu, P. *Chem. Phys. Lett.* **1978**, *57*, 220.
(32) Sobolewski, A. L. *Photochem. Photobiol.* **1995**, *89*, *89.*
(33) Hirst, J. D.; Hirst, D. M.; Brooks III, C. L. *J. Phys. Chem.* **1996**, *100*, 13487.
(34) Li, Y.; Garrell, R.-L-; Houk, K. N. *J. Am. Chem. Soc*. **1991**, *113*, 5895.
(35) Turro, N. J. *Modern Molecular Photochemistry*; Benjamin/Cummings: Menlo Park, CA, 1978.
(36) Frisch, M. J.; Trucks, G. W.; Schlegel, H. B.; Gill, P. M. W.; Johnson, B. G.; Robb, M. A.; Cheeseman, J. R.; Keith, T.; Petersson, G. A.; Montgomery, J. A.; Raghavachari, K.; Al-Laham, M. A.; Zakrzewski, V. G.; Ortiz, J. V.; Foresman, J. B.; Cioslowski, J.; Stefanov, B. B.; Nanayakkara, A.; Challacombe, M.; Peng, C. Y.; Ayala, P. Y.; Chen, W.; Wong, M. W.; Andres, J. L.; Replogle, E. S.; Gomperts, R.; Martin, R. L.; Fox, D. J.; Binkley, J. S.; Defrees, D. J.; Baker, J.; Stewart, J. P.; Head-Gordon, M.; Gonzalez, C.; Pople, J. A. GAUSSIAN 94; Revision B.1; Gaussian Inc.: Pittsburgh, PA, 1995.
(37) Møller, C.; Plesset, M. S. *Phys. Rev.* **1934**, *46*, 618.
(38) Binkley, J. S.; Pople, J. A. *Int. J. Quantum Chem.* **1975**, *9*, 229.
(39) Becke, A. D. *J. Chem. Phys.* **1993**, *98*, 1372.
(40) Becke, A. D. *J. Chem. Phys.* **1993**, *98*, 5648.
(41) Becke, A. D. *Phys. Rev. A* **1988**, *38*, 3098.
(42) Lee, C.; Yang, W.; Parr, R. G. *Phys. Rev. B* **1988**, *37*, 785.
(43) Johnson, B. G.; Gill, P. M. W.; Pople, J. A. *J. Chem. Phys.* **1993**, *98*, 5612.
(44) Foresman, J. B.; Head-Gordon, M.; Pople, J. A.; Frisch, M. *J. Phys. Chem.* **1992**, *96*, 135.
(45) McLean, A. D.; Chandler, G. S. *J. Chem. Phys.* **1980**, *72*, 5639.
(46) Krishnan, R.; Binkley, J. S.; Seeger, R. S.; Pople, J. A. *J. Chem. Phys.* **1980**, *72*, 650.
(47) Clark, T.; Chandrasekhar, J.; Spitznagel, G. W.; Schleyer, P.v. R. *J. Comput. Chem.* **1983**, *4*, 294.
(48) Frisch, M.; Pople, J. A.; Binkley, J. S. *J. Chem. Phys.* **1984**, *80*, 3265.
(49) Dubost, H. *Chem. Phys.* **1976**, *12*, 139.
(50) Hagen, W.; Tielens, A. G. G. M. *Spectrochim. Acta* **1982**, *38A*, 1103.
(51) Fraser, G. T.; Nelson Jr., D. D.; Peterson, K. I.; Klemperer, W. *J. Chem. Phys*. **1986**, *84*, 2472.
(52) Lundell, J.; Krajewska, M.; Räsänen, M. *J. Mol. Struct.*, in press.
(53) Süzer, S.; Andrews, L. *J. Chem. Phys.* **1987**, *87*, 5131.
(54) Abouaf-Marguin, L.; Jacox, M.; Milligan, D. E. *J. Mol. Spectrosc.* **1977**, *67*, 34.
(55) Okabe, H. *Photochemistry of Small Molecules*, Wiley-Interscience: New York, 1978.
(56) Lundell, J.; Räsänen, M. *J. Phys. Chem.* **1995**, *99*, 14301.
(57) Lundell, J.; Räsänen, M. *J. Mol. Struct.* **1997**, *436*−*437*, 349.
(58) Milligan, D. E.; Jacox, M. E. *J. Chem. Phys.* **1964**, *40*, 2457.
(59) Bondybey, V. E.; English, J. M.; Mathews, C. W.; Contolini, R. J. *J. Mol. Spectrosc.* **1982**, *92*, 431.
(60) Teles, J. H.; Maier, G.; Hess Jr., B. A.; Schaad, L. J.; Winnewisser, M.; Winnewisser, B. P. *Chem. Ber.* **1989**, *122*, 753.
(61) Pettersson, M.; Lundell, J.; Räsänen, M. *J. Chem. Phys.* **1995**, *103*, 205.
(62) Kunttu, H.; Seetula, J.; Räsänen, M.; Apkarian, A. P. *J. Chem. Phys.* **1992**, *96*, 5630.
(63) Schriever, R.; Chergui, M.; Schwentner, N. *J. Phys. Chem.* **1991**, *95*, 6124.
(64) Kunttu, H.; Dahlqvist, M.; Murto, J.; Räsänen, M. *J. Phys. Chem.* **1988**, *92*, 1495.
(65) Morgan, M. A.; Pimentel, G. C. *J. Phys. Chem.* **1989**, *93*, 3056.
(66) Zhang, J.; Dulligan, M.; Wittig, C. *J. Phys. Chem.* **1995**, *99*, 7446.
(67) Lundell, J.; Krajewska, M.; Räsänen, M., unpublished results.